Groundwater

Continental Scale Hydrostratigraphy: Comparing Geologically Informed Data Products to Analytical Solutions

by Jackson S. Swilley[1], Danielle Tijerina-Kreuzer[1], Hoang V. Tran[1,2], Jun Zhang[3,4], Chen Yang[1], Laura E. Condon[4], and Reed M. Maxwell[1,5,6]

Abstract

This study synthesizes two different methods for estimating hydraulic conductivity (K) at large scales. We derive analytical approaches that estimate K and apply them to the contiguous United States. We then compare these analytical approaches to three-dimensional, national gridded K data products and three transmissivity (T) data products developed from publicly available sources. We evaluate these data products using multiple approaches: comparing their statistics qualitatively and quantitatively and with hydrologic model simulations. Some of these datasets were used as inputs for an integrated hydrologic model of the Upper Colorado River Basin and the comparison of the results with observations was used to further evaluate the K data products. Simulated average daily streamflow was compared to daily flow data from 10 USGS stream gages in the domain, and annually averaged simulated groundwater depths are compared to observations from nearly 2000 monitoring wells. We find streamflow predictions from analytically informed simulations to be similar in relative bias and Spearman's rho to the geologically informed simulations. *R*-squared values for groundwater depth predictions are close between the best performing analytically and geologically informed simulations at 0.68 and 0.70 respectively, with RMSE values under 10 m. We also show that the analytical approach derived by this study produces estimates of K that are similar in spatial distribution, standard deviation, mean value, and modeling performance to geologically-informed estimates. The results of this work are used to inform a follow-on study that tests additional data-driven approaches in multiple basins within the contiguous United States.

Introduction

While groundwater is the world's largest accessible freshwater resource, it is intrinsically difficult to characterize. Direct observations of groundwater can only be made using a limited number of approaches, primarily monitoring wells, which are restrictive in scale. Remote sensing has been used to create global-scale soil moisture products like Soil Moisture Active Passive (SMAP) and Soil Moisture and Ocean Salinity mission (SMOS); however, these products are most accurate up to 5 cm in depth and lend themselves better to land-surface applications than groundwater availability applications (Jackson et al. 2012; Velpuri et al. 2015; O'Neill et al 2020). Coarse estimates of groundwater anomalies can be made using remote sensing products like GRACE (the Gravity Recovery and Climate Experiment), but these estimates are made over large scales on the order of $10^2 - 10^4\ km^2$ (Tapley et al. 2004; Scanlon et al. 2018). Management of this vital resource is made even more challenging by the complex interrelation of groundwater with unsaturated zone soil moisture, surface water, and even the lower atmosphere (Maxwell and Condon 2016; Forrester and Maxwell 2020).

Hydrogeologic properties are similarly hard to observe. Hydraulic conductivity (K) is typically inferred in groundwater models using a calibration or parameter estimation approach (Hill and Tiedeman 2007). While common practice for more local to regional systems, calibration approaches are still computationally

[1]Department of Civil and Environmental Engineering, Princeton University, Princeton, NJ
[2]Pacific Northwest National Laboratory, Richland, WA
[3]Key Laboratory of VGE of Ministry of Education, Nanjing Normal University, Nanjing, China
[4]Hydrology and Atmospheric Sciences, University of Arizona, Tucson, AZ
[5]The High Meadows Environmental Institute, Princeton University, Princeton, NJ
[6]Corresponding author: Department of Civil and Environmental Engineering, Princeton University, Princeton, NJ; reedmaxwell@princeton.edu

Article impact statement: Analytical approaches can estimate hydraulic conductivity fields that perform comparably to datasets derived from geologic maps.

Received January 2023, accepted September 2023.

doi: 10.1111/gwat.13354

impractical at large scales (Zell and Sanford 2020; Condon et al. 2021; Gleeson et al. 2021). Developing an accurate subsurface architecture becomes even more important given the uncertainties and that alternate subsurface representations are rarely explored (Enemark et al. 2019, 2020). Integrated hydrologic models simulate surface and subsurface flow simultaneously. They can be used in a predictive sense and to connect information from disparate observations like groundwater wells and stream gages. For example, Foster et al. (2020) used numerical experiments to find that low-resolution models may underpredict the effects of climate change on mountain headwater streamflows, and Forrester and Maxwell (2020) used scenario testing to determine how lateral groundwater flow affects evapotranspiration in complex terrain. Continental-scale models are essential in many cases, as some of the processes governing the hydrologic cycle, as well as many perturbations to the hydrologic cycle, function at large scales (Eagleson 1986; Barthel 2014; Bierkens et al. 2015).

Physically based hydrologic models require the properties of the domain being simulated. K is a critical input to any subsurface model (Freeze and Cherry 1979). This subsurface parameter is important for accurate numerical modeling of groundwater systems and is a key component of the analytical equations of groundwater flow as well. For modeling, an accurate 3D gridded representation of hydraulic conductivity is important for model performance (Turner 1992). As mentioned above, calibration of hydraulic conductivity is a standard practice in groundwater modeling, but computational demand makes the calibration of high-resolution, continental-scale models to groundwater head or water table depths (WTD) and streamflow simultaneously, infeasible (Condon et al. 2021; Gleeson et al. 2021; O'Neill et al. 2021). A common approach has been to assemble subsurface properties based on large scale datasets (e.g., Huscroft et al. 2018; de Graaf et al. 2020), however newer approaches are evolving that are semi-analytical (e.g., Luo et al. 2010; Tashie et al. 2021) that provide an alternate pathway to populating hydraulic conductivity values.

Our study develops and compares multiple continental-scale hydraulic conductivity spatial models for the contiguous United States using two steps. The first step is a mapping component in which several methods are used to estimate the saturated subsurface hydraulic conductivity of the contiguous United States and adjacent hydrologic regions. These include existing datasets, new combinations of existing data products and analytical solutions for hydraulic conductivity calculated based on different assumptions. The second component of our analysis is to evaluate how each hydraulic conductivity map influences the performance of an integrated hydrologic model for an example test domain. We use selected 3D K fields as input to a ParFlow-CLM integrated hydrologic model that simulates surface water and groundwater simultaneously for a major U.S. river basin, the Upper Colorado. Modeling results are compared to observed streamflow and WTD for each subsurface data product. This process assesses the performance of the hydraulic conductivity fields themselves and the approaches used to develop them and their underlying assumptions.

Understanding Hydraulic Conductivity

The challenge of mapping hydraulic conductivity lies in the inability to observe it completely. Unlike hydrologic features such as topography or stream density, hydraulic conductivity cannot currently be observed or inferred using remote sensing techniques. Adding to this challenge is the fact that hydraulic conductivity can vary by 10 orders of magnitude or more between differing subsurface media (Heath 1983), and the boundaries of these subsurface media are difficult to map at high spatial resolution. Although K can be measured directly in a lab using core samples or in situ using slug and pump tests, these methods are restrictive in scale and can be expensive (Hornberger et al. 1998). Lab testing core samples measures the conductivity of a single point in space at a very small support scale, meaning that the effects of subsurface heterogeneity go largely unaccounted. While slug and pump tests directly measure the effective hydraulic conductivity of real groundwater systems, their results are only representative of the nearby subsurface on the order of meters to hundreds of meters (Hornberger et al. 1998).

Hydraulic conductivity, when mapped at continental and global scales, is often assigned by subsurface hydrogeology (Gleeson et al. 2014; Huscroft et al. 2018). This approach finds the best available mapping of geology for a region and assigns a value of K for each geological unit. We will refer to this type of approach as geologically informed throughout. The factor that determines the accuracy of this approach is often data availability—in regions where geology is mapped closely, K can be mapped similarly. One advantage of geologically informed approaches is that they can be performed efficiently over large areas when the geology has been mapped and it allows for local calibration and/or smaller-scale subdivision of these geologic units.

Analytical approaches to estimating K leverage assumptions on groundwater flow to work backwards from observed hydrology to subsurface hydraulic properties. The advantage of these approaches is that they may capture the effective hydraulic conductivity at the scale of interest. This means that they would, ideally, capture the effect of features like faults, karst, and fracture systems at scale; however, this is untested in practice. Additionally, they do not suffer from discontinuities at administrative boundaries, which are sometimes found in geology maps.

A methodology developed by Luo and colleagues is an analytical K estimation approach that uses the geomorphology and hydrology of a domain (Luo et al. 2010; Luo and Pederson 2012). We provide details on the application of this approach below but summarize briefly here. Streams are assumed to be gaining, meaning that they

receive baseflow from groundwater, and the density of streams in a domain is assumed to negatively correlated to the permeability of that domain (Pederson 2001; Luo et al. 2010). This approach assumes that catchments are generally in steady-state when considering the long-term averages of recharge and spring flows. Using this assumption, a mass balance can be performed over a catchment, and hydraulic conductivity can be estimated by making the DuPuit-Forchheimer assumptions and rearranging the groundwater equation (Luo et al. 2010). This approach, and similar approaches, represents promise as they address the problem of effective K versus local K. They also represent efficient methods for estimating hydraulic conductivity at large scales. To our knowledge, no study has evaluated the results of such methods with an integrated hydrologic model.

In addition to relating hydraulic conductivity with stream density, our study also assumes a relationship between topography and the water table of unconfined aquifer units. The relationship between topography and the water table of unconfined aquifers has been recognized since the 19th century (King 1899). It is commonly said in hydrology that the water table behaves as a "subdued replica of the ground surface," and we will use this principal to equate large-scale averages in topographic slope to average hydraulic gradient (Desbarats et al. 2002). There remains, however, some question over how and when this relationship can be used. Desbarats et al. (2002) explains the advantages and challenges of relating topography and groundwater elevation in application when producing two models to map groundwater depth using a digital elevation model. Haitjema and Mitchell-Bruker (2005) discuss the circumstances under which water tables are topography controlled and conversely recharge controlled, but ultimately conclude that there is nearly always some degree of correlation at large scales.

We will use Luo's approach as an example of an analytical approach from literature and Huscroft's GLHYMPS 2.0 data product as an example of a geological K mapping from literature. It is important, however, to acknowledge approaches that we do not consider in our analysis. There are many continental and global-scale K products that make use of pedotransfer functions to estimate hydraulic properties of soil from more easily measurable properties (e.g. Gupta et al. 2021; Jarvis et al. 2013; Montzka et al. 2017; Rahmati et al. 2018). These approaches could be considered a subcategory of geologically informed approaches. We choose not to include a pedotransfer approach or product because their focus is on shallower soil units, and ours is up to 1.2 km of subsurface hydrostratigraphy. We have also not included the Tashie et al. (2021) analytically informed K data products who use hydrograph recession analysis to estimate the watershed-scale effective hydraulic conductivity of the contiguous United States, or the shallow calibrated transmissivities of Zell and Sanford (2020), both of which were not available when this work was being undertaken and are for shallower systems than we consider in this work.

Methods

Our process for this study begins with using several methods to map saturated subsurface hydraulic conductivity for the contiguous United States. We categorize these approaches as *geological*, meaning that K is assigned based on knowledge of the subsurface geology and *analytical*, meaning that they rely on a mathematical formulation. We create six hydraulic conductivity maps using an analytical approach from literature; we create six more maps using an analytical approach derived in this study, and we compare with three geologically-derived maps; two of which were compiled or edited for this study, and a third which was taken directly from literature. These two-dimensional products are then combined into a 3D K field. We discuss and evaluate the statistics of the K fields derived from these different approaches.

These three-dimensional K fields are then used as subsurface inputs to the integrated hydrological model, ParFlow-CLM of the Upper Colorado River Basin (UCRB) to evaluate how each mapping influences model performance. ParFlow-CLM simulates surface water and groundwater simultaneously and is driven by hourly atmospheric forcing for an entire water year. Simulated daily streamflows are compared to daily flow data from 10 USGS stream gages in the domain, and annually averaged simulated groundwater depths are compared to observations from nearly 2000 monitoring wells. We would like to emphasize here that this test basin is intended only to illustrate the ways that different K data products can influence model behavior. This is not indented to be an exhaustive national modeling study.

We perform all mapping analyses over the contiguous United States and areas outside the United States connected to major U.S. river basins. Figure 1 provides an outline of the full study area with the UCRB modeling subdomain delineated in black. This spatial extent was chosen to include all areas that drain to United States, such as the Columbia River Basin and the full Rio Grande Basin, for future modeling efforts. Mapping is done in 2D at high resolution with grid cells of 1 km^2. Analytical approaches average hydrologic parameters of a catchment at the U.S. Geological Survey (USGS) Hydrologic Unit Code, HUC12 scale; HUC12s are watershed areas mapped by the USGS on the order 10^2 km^2 on average. Geologically informed K maps, those with vector geometry originally, are rasterized at the aforementioned one-kilometer resolution as are the borders of the HUC12 catchments. Table 1 provides a full list of the hydraulic conductivity products considered in this study.

Geological Methods

The geologically informed maps use existing datasets to assign K values (Figure 2, Table 1). The first of the geologically informed data products is the GLHYMPS 2.0 dataset from Huscroft et al. (2018), referred to from here forward as *Geological K Case 1*. This product is composed of two vertical layers, with the top layer extending from the surface to an estimated depth of bedrock provided by Shangguan et al. (2017) and the second layer

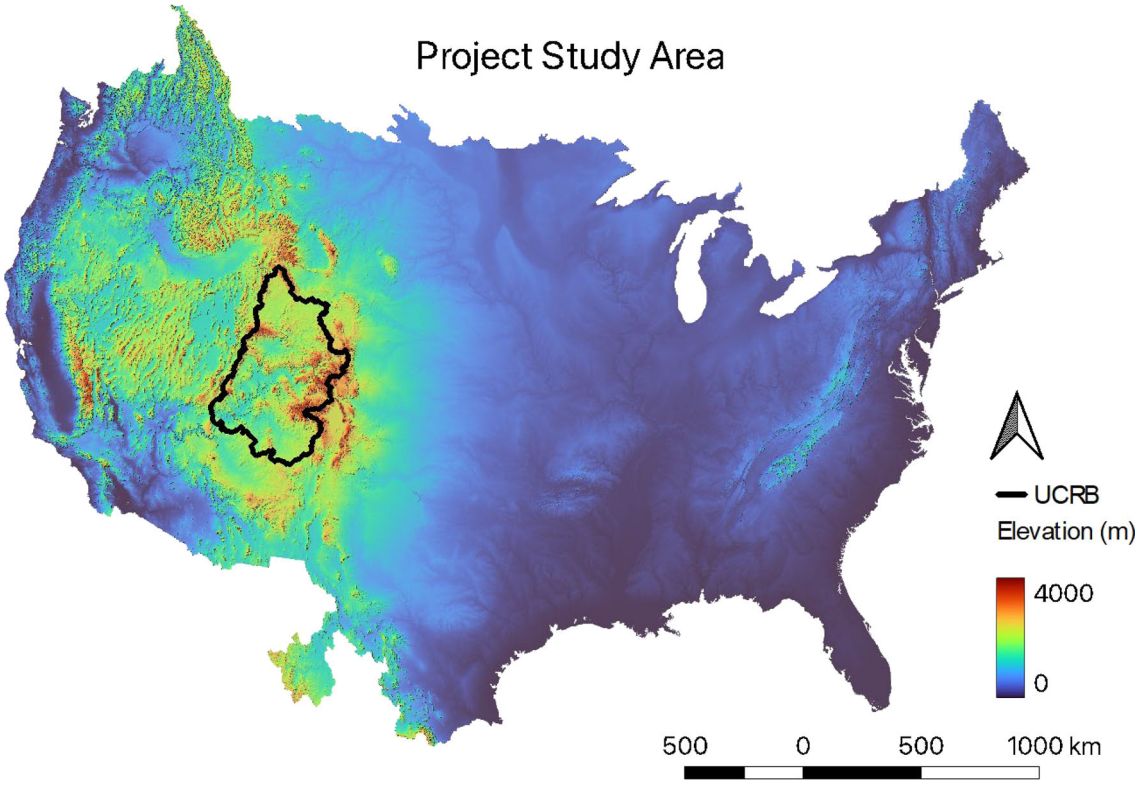

Figure 1. Hydraulic conductivity mapping domain with modeling subdomain: the contiguous United States and inward-flowing watersheds and the Upper Colorado River Basin (UCRB).

beneath. The upper layer predominantly represents unconsolidated areas, while the lower layer predominantly represents the underlying geology (Huscroft et al. 2018). It is important to note that these layers are properties of the dataset itself, independent of model layers. When applying the dataset to our modeling application, we assign properties of the top layer to cells with centers above Shangguan's estimate of depth to bedrock and properties of the bottom layer to cells with centers beneath it. A depiction of this vertical disaggregation can be seen in Figure 3.

The second geologically informed data product is created by assigning K values from Heath (1983) to a geology map created by the USGS (Belitz et al. 2019). This K field will be referred to as *Geological K Case 2* mapping hereinafter. The USGS geology map used is the union of the USGS Principal Aquifer dataset and Secondary Hydrogeologic Regions dataset (Belitz et al. 2019). Combined, these two maps cover the entirety of the United States. Outside of U.S. borders, *Geological K Case 1* geology values are used.

Our study considers a third geology-informed data product for comparison. This K field uses the geometries from *Geological K Cases 1* and *2* but assigns estimates of K from Maxwell et al. (2015) to each rock type. Described in detail in Maxwell et al. (2015), these values are a combination of the Gleeson et al. (2011) values and other literature values. This is a two-layer product—the upper layer is the top layer of the *Geological K Case 1* map, and the bottom layer is the *Geological K Case 2* geometry. As in *Geological K Case 1*, the top layer is mapped down to the Shangguan estimated depth of bedrock. The idea supporting this approach is that the top layer of *Geological K Case 1* focuses on the unconsolidated, near-surface units, and *Geological K Case 2* focuses on deeper units. Unconsolidated areas are mapped as bedrock in the lower layer below the depth to bedrock product. This is done because the underlying dataset is vertically-averaged, and unconsolidated areas are expected to be accounted for by *Geological K Case 1* in the upper layer. We will refer to this product as *Geological K Case 3*. All K fields are summarized in Table 1.

Analytical Methods

As mentioned previously, we use two analytical approaches in this study. Using these two analytical approaches with different assumptions, we create and assess a total of 12 mappings—9 for actual hydraulic conductivity (L/T) and 3 for transmissivity (L/T^2)—based on the combination of analytical approach and assumptions (Table 1) and input data (Figures S1 through S6).

The first analytical approach that we implement was developed by Luo et al. (2010). From here forward, this approach will be referred to as the *Literature Analytical Approach*. This method starts with the conceptual diagram shown in Figure 4, develops an equation for steady-state flux to the stream and inverts for hydraulic conductivity. Luo et al. (2010) and Luo and Pederson (2012) derive this

Table 1
Summary and Description of Subsurface Data Products and the Resulting K Fields

Name	Layers	Method	Assumptions
Geological K Case 1 (K Case G1)	2	K values from Huscroft et al. (2018); Shangguan depth to bedrock (2016)	NA
Geological K Case 2 (K Case G2)	1	USGS Primary Aquifers and Secondary Hydrologic Regions assigned K values by this study	NA
Geological K Case 3 (K Case G3)	2	GLYMPS 2.0 geometry over USGS Primary Aquifer geometry assigned K by this study; Shangguan depth to bedrock (2016)	ParFlow Indicators
Analytical K Case 1 (K Case A1)	1	Literature analytical method (Luo et al. 2010) with drainage density and aquifer depth (H) larger than 100 m	H ≥ 100 m
Analytical K Case 2 (K Case A2)	1	Literature analytical method (Luo et al. 2010) with drainage density and valley depth (d) limited to aquifer depth	d ≤ H
Analytical K Case 3 (K Case A3)	1	Literature analytical method (Luo et al. 2010) with drainage density and aquifer depth (H) set to a constant value	H = 200 m
Analytical K Case 4 (K Case A4)	1	Literature analytical method (Luo et al. 2010) with average effective flow length (same as Case A1 above but with effective flow length)	H ≥ 100 m
Analytical K Case 5 (K Case A5)	1	Literature analytical method (Luo et al. 2010) with average effective flow length (same as case A2 but with effective flow length)	d ≤ H
Analytical K Case 6 (K Case A6)	1	Literature analytical method (Luo et al. 2010) with average effective flow length (same as case A3 but with effective flow length)	H = 200 m
Analytical K Case 7 (K Case A7)	1	This study's analytical method using average effective flow length	NA
Analytical K Case 8 (K Case A8)	1	This study's analytical method using drainage density	NA
Analytical K Case 9 (K Case A9)	1	This study's analytical method using average effective flow length	Model slopes and flow lengths
Analytical T Case 1 (T Case A1)	1	This study's analytical method using average effective flow length	NA
Analytical T Case 2 (T Case A2)	1	This study's analytical using drainage density	NA
Analytical T Case 3 (T Case A3)	1	This study's analytical method using average effective flow length	Model slopes and flow lengths

equation for flux based on the Dupuit equation. We briefly rederive the Luo et al. (2010) formulation here starting from Darcy's law combined with a simple statement of continuity. If we start with the Darcy equation:

$$q' = -Kb\left(\frac{\Delta h}{\Delta x}\right) \tag{1}$$

Where K is the effective hydraulic conductivity [L/T], h is the hydraulic head [L], x is a distance along the hillslope, b is the average aquifer thickness expressed as $b = \frac{(H-(H-d))}{2}$, and q' is the flux from *both* hillslopes that drain into the stream as shown. If we assume no underflow (or inter-basin flow) from neighboring hillslopes, we can say that $q' = 2RW$ where R is the effective recharge [L/T], W is the length from hilltop to stream [L] and the factor of two appears because q' represents the flow from both hillslopes shown in Figure 4. H is the aquifer thickness [L], assumed to be from the bedrock to the top of the hillslope and d is the valley depth [L], or the change in elevation or topography from the top of the hillslope to the stream.

The change in head in (1) may be written as $\Delta h = (h - d) - H$ [L] and the distance becomes $\Delta x = W$ [L]. If we combine and simplify we get:

$$2RW = \frac{K}{2W}\left(H^2 - (H-d)^2\right) \tag{2}$$

When we solve (2) for K we get:

$$K = \frac{4RW^2}{\left(H^2 - (H-d)^2\right)} \tag{3}$$

Which is the same as Equation 2 in Luo and Pederson (2012). Note that this same solution is obtained using the Dupuit derivation and setting the constants of integration based on the system as shown in Figure 4. This analytical solution assumes that catchments are effectively drained, aquifer thickness is equal to depth-to-bedrock,

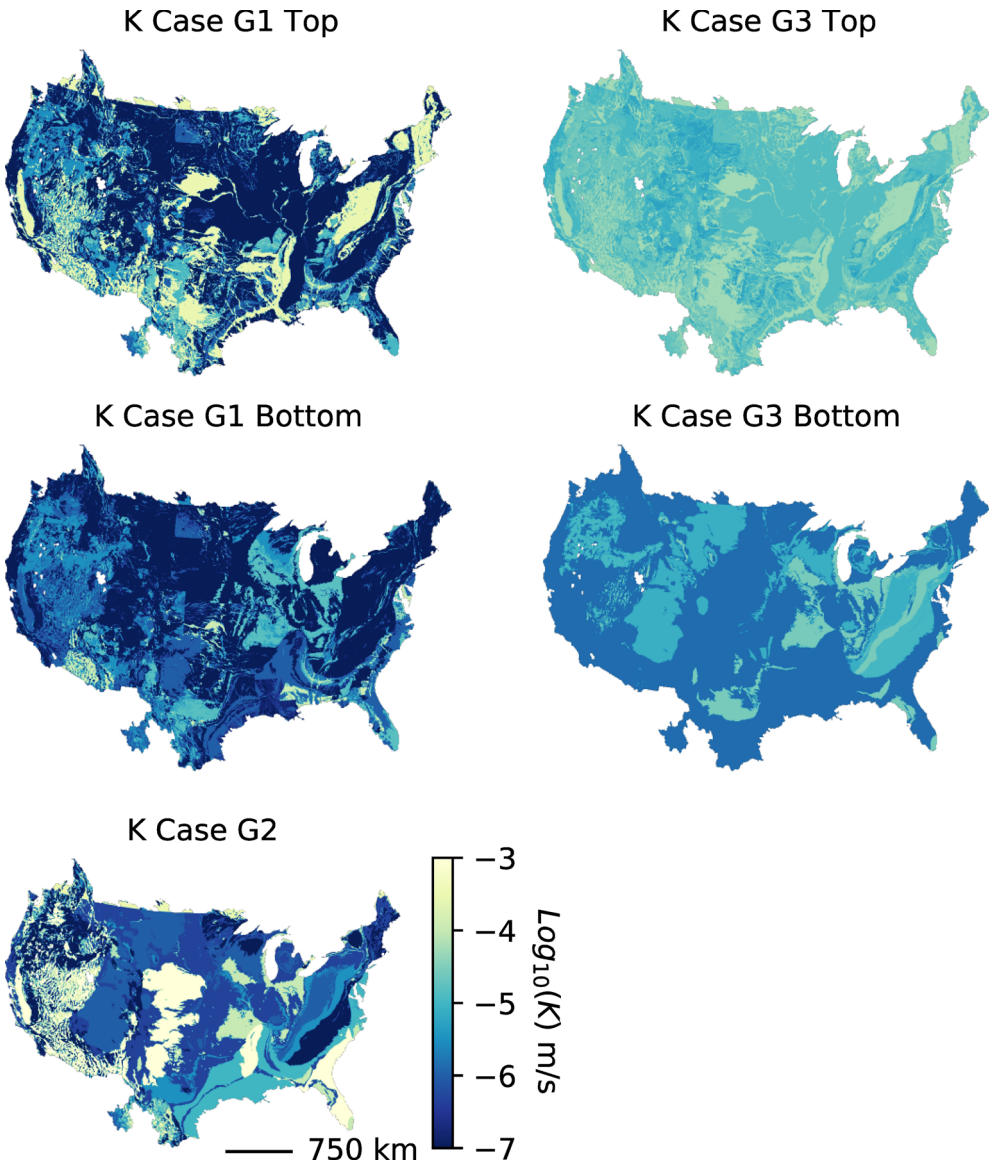

Figure 2. Geologically informed hydraulic conductivity data products. See Table 1 for definitions.

and groundwater flow is horizontal. As the length from hilltop to stream is not always easily determined, the drainage density [L^{-1}] may be used in place of W.

Drainage density (D), while not depicted in Figure 4, is roughly equivalent to $1/2W$, where W is the average flow length to the nearest stream for water that falls in a catchment (Luo et al. 2010). D can be estimated by dividing the total length of streams in a catchment by the catchment's area. W can be calculated by averaging the downstream distance from every location in a watershed to the nearest stream. If drainage density is used then Equation 3 becomes:

$$K = \frac{R}{D^2\left[H^2 - (H-d)^2\right]} \tag{4}$$

Both terms, D and W, will be tested by our analytical K cases. These parameters are derived using the National Hydrography Dataset (NHD) Plus stream map (U.S. Geological Survey 2019). Parameters such as: recharge, aquifer thickness, valley depth, and drainage density, are averaged over each USGS HUC12 catchment (U.S. Geological Survey 2019). These parameters are used in Equation 4 to estimate K for each catchment and are illustrated in Figure 4.

Hydraulic gradient is assumed to be a function of aquifer thickness and valley depth, which is defined as the average depth of erosion along streams. Valley depth can be approximated by taking the black top hat transform of a digital elevation model (Rodriguez et al. 2002). This study performs the black top hat transform at ~30 m resolution over the entire contiguous United States, as shown in Figure S5. The resulting black top hat transform is then averaged at 250 m resolution for storage and use. To convert this 250 m black top hat product to valley depth, it is then averaged along the NHD streams for each catchment.

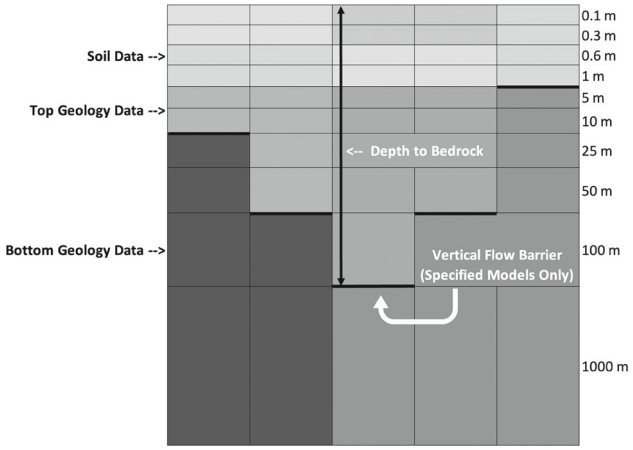

Figure 3. Conceptual model of 3D hydraulic conductivity and vertical discretization of test domain (not drawn to scale). Note that certain features identified here may change depending on the case simulated such as the presence of the flow barrier as described in Table 3, or the discrete nature of K values for the *Geological* cases.

Aquifer thickness is assumed to be equivalent to the depth of bedrock. This means that the *Literature Analytical Approach* assumes that unconsolidated areas are fully saturated some distance away from their draining streams and that bedrock geologies do not contribute to baseflow. Further assumptions on the value of aquifer thickness and valley depth are necessary as well in this approach. The mathematical formula of the *Literature Analytical Approach* produces negative hydraulic conductivities when valley depth is more than twice aquifer thickness. We test three assumptions that remedy this problem: (1) assuming aquifer thickness is greater than or equal to 100 m; (2) assuming valley depth is less than or equal to aquifer thickness; (3) assuming aquifer thickness is a constant 200 m. These assumptions are outlined in Table 1. Finally, recharge was estimated by subtracting average evapotranspiration from precipitation (Tran et al. 2020). These two parameters were averaged over each catchment for calculation.

The second analytical approach, which is first proposed in the current study, is a variation of the Luo's method where the hydraulic gradient is assumed to be equivalent to topographic slope (Zhang et al. 2021). This new formulation alleviates the need for the additional assumptions on aquifer thickness and valley depth. This study's approach is used for the creation of both hydraulic conductivity sets and transmissivity (T) sets. The formulas for these methods are provided below by Equations 5 and 6. For two cases, one K and one T, slopes and flow lengths from the UCRB ParFlow model were used instead of the true landscape slopes and flow lengths to assess the importance of inner consistency when modeling permeabilities.

$$K = -\frac{RW}{SH} \tag{5}$$

$$T = -\frac{RW}{S} \tag{6}$$

K—hydraulic conductivity (L/T).
T—transmissivity (L^2/T).
R—average recharge (L/T).
W—effective flow length (L).
H—aquifer thickness (L).
S—topographic slope (L/L).

In some areas of our domain, we did not have sufficient data for one or more of the required input parameters. Gaps in the input data hampered the application of the analytical solutions in these regions, primarily in HUC12s with limited NHD Plus stream data. To address this, we implement two data filling techniques. No-data areas inside of U.S. borders are filled using simple nearest neighbor interpolation for smoothness. No-data areas outside of the U.S. borders, which are larger on average, are extrapolated using a linear ridge model from Scikit Learn (Pedregosa et al. 2011). For both hydraulic conductivity and transmissivity, the extrapolation model is trained on recharge and elevation, as our analytical solutions are sensitive to both of these parameters. Table 2 shows the percentages of the domain interpolated and extrapolated for each analytical case.

Modeling Methods

The UCRB is approximately 284,898 km^2 in area and covers portions of Wyoming, Colorado, Utah,

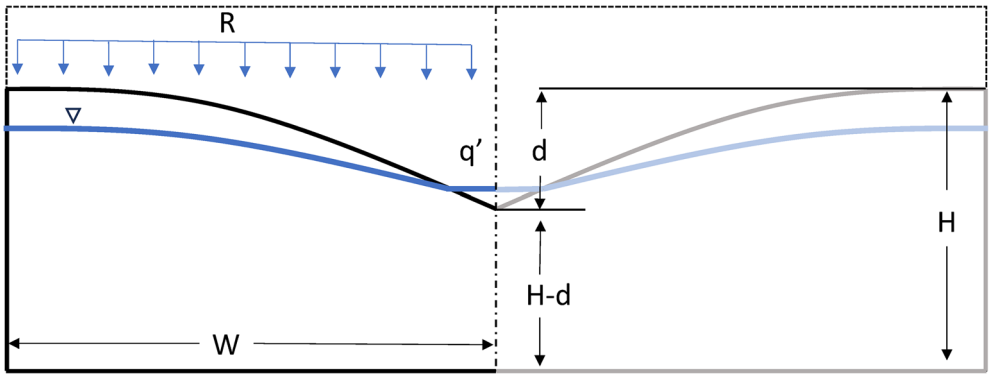

Figure 4. Conceptual model of hydrologic catchment properties modified after (Luo et al. 2010).

Table 2
Percentages of Domain Interpolated and Extrapolated

K Field	Interpolation %	Extrapolation %	Total %
Analytical K Case 1	15.79	5.72	21.51
Analytical K Case 2	16.18	5.72	21.90
Analytical K Case 3	15.77	5.72	21.49
Analytical K Case 4	15.88	5.72	21.60
Analytical K Case 5	17.00	5.72	22.72
Analytical K Case 6	15.83	5.72	21.55
Analytical K Case 7	2.63	5.72	8.35
Analytical K Case 8	15.78	5.72	21.50
Analytical K Case 9	3.06	5.72	8.78

New Mexico, and Arizona (Figure 1). It encompasses high-elevation mountain headwaters, lower prairie land and even deserts, making it hydrologically diverse. The UCRB is also topographically constrained and large in extent, meaning that the lateral flow through the edges of the domain are much smaller than other subbasins. The UCRB also has a range of topography and a mix of rain and snow processes across its extent. Despite the water management present in this system (which was not considered in the simulations) we still felt this was an optimal choice as a test domain. Modeling is performed for the water year of 1983 in the UCRB. The water year chosen and UCRB domain are advantageous as there is clear seasonality in flow regimes due to snow melt allowing baseflow and peak flows to be analyzed separately. We use this opportunity to disentangle the surface water controls of subsurface hydraulic conductivity (e.g., Foster and Maxwell 2019). The dramatic snowmelt-driven peak flows of 1983 also allow us to observe model performance in extreme conditions.

The model used for simulations is ParFlow-CLM, a 3D integrated hydrologic model, coupled to the land surface model, CLM (Ashby and Falgout 1996; Jones and Woodward 2001; Maxwell and Miller 2005; Kollet and Maxwell 2006, 2008; Maxwell 2013). The UCRB is modeled at 1 km horizontal resolution and varying vertical resolution; the vertical discretization can be seen in Figure 3. CLM, a land surface model, is used in all simulations, and hourly NLDAS meteorological forcing for the water-year of 1983 drives meteorological inputs (Xia et al. 2014). Eight meteorological variables (wind, two component solar, pressure, temperature, precipitation, humidity) were bilinearly interpolated to each grid cell to create this forcing dataset which was then used to drive the CLM portion of ParFlow-CLM. Each simulation case was spun up using a two-step approach, first a steady state P-ET forcing product followed by 2 years of transient simulation. Soil data from STATSGO2 makes up the first 2 m of each model domain, with our hydraulic conductivity fields beneath (Figure 3) (Soil Survey Staff n.d.). An additional advantage of Geological K Case 3 is that the soil layers have spatially variable porosities

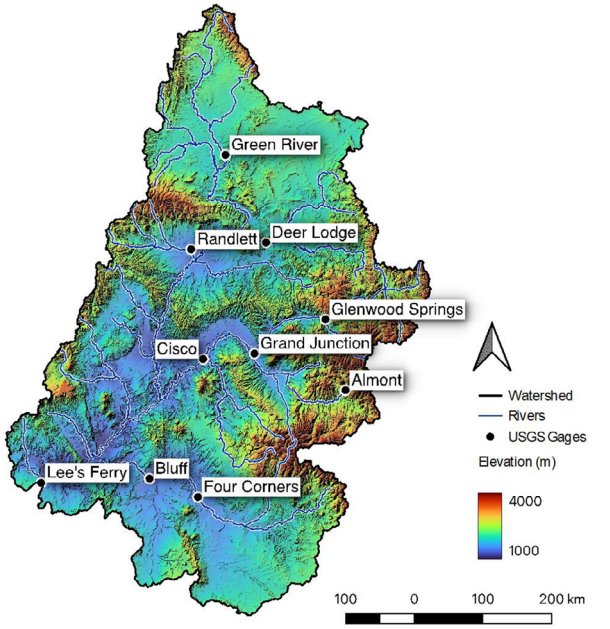

Figure 5. Model domain: Upper Colorado River Basin above Lee's Ferry.

and van Genuchten water retention properties. These properties are associated with the geologic indicators in ParFlow-CLM used in this test case, documented by Condon and Maxwell (Condon and Maxwell 2013; Condon and Maxwell 2014).

Modeled stream flows are compared to observed flows from USGS stream gages at 10 locations in the UCRB (Figure 5). We take an unweighted arithmetic mean of streamflow at USGS gage points so that headwaters have suitable representation. Simulated WTD is compared to observation well data (Fan et al. 2013). In this comparison, WTD is calculated as a free water table below the ground surface, averaged over the water year, which is consistent with the Fan et al. (2013) database.

We ran a total of 10 simulations beginning with one K case from each analytical approach and our three geological K maps for comparison. After concluding the first five simulations, we moved forward with an additional five simulations; this time making use of a model element referred to as a vertical flow barrier, which simulates confining units by reducing flow at specified model cell interfaces (Marshall et al. 2022). The depth at which the vertical flow barrier is applied can be constant or can vary laterally (see Figure 3). We apply the flow barrier to reduce, but not eliminate, vertical flow between simulated deeper groundwater systems and the unconfined upper units that typically interact more dynamically with surface water. For four analytical cases, we apply the vertical flow barrier at the depth that was used to define the aquifer thickness when calculating K thus reducing the transmissivity of the simulated unconfined upper aquifer to the same as was implied by the approach. We also ran a simulation using the *Geological K Case 1* product combined with a vertical flow barrier at Shangguan's estimate of depth to bedrock for comparison. Table 3

Table 3
Modeling Simulations

Subsurface	Vertical Flow Barrier Depth
Geological K Case 1	Vertical flow barrier not used
Geological K Case 2	Vertical flow barrier not used
Geological K Case 3	Vertical flow barrier not used
Analytical K Case 1	Vertical flow barrier not used
Analytical K Case 7	Vertical flow barrier not used
Geological K Case 1	Variable-depth flow barrier: SFBZ
Analytical K Case 1	(modified) Variable-depth flow barrier: mSFBZ
Analytical K Case 7	Variable-depth flow barrier: SFBZ
Analytical K Case 3	Constant, 192 m-depth flow barrier: CFBZ
Analytical T case 1	Constant, 192 m-depth flow barrier: CFBZ

Notes: CFBZ indicates a constant-depth flow barrier and SFBZ indicates a variable-depth flow barrier at Shangguan's depth to bedrock. The modified variable-depth flow barrier (mSFBZ) is located at a depth of 100 m or Shangguan's estimate of depth to bedrock, whichever is greater.

provides a full list of the modeling simulations run and the method of assigning a vertical flow barrier.

Results

Hydraulic Conductivity Data Product Results

We evaluate six hydraulic conductivity data products using the *Literature Analytical Approach*, and three hydraulic conductivity solutions and three transmissivity solutions for the using *this study's analytical approach*. The spatial distribution of K in five representative hydraulic conductivity products can be seen in Figure 6. We see the two analytical approaches produce K maps that are very similar in value and spatial distribution. When comparing geological K maps with analytical maps, a few features are present in all. This includes the Mississippi Embayment and California's Central Valley; the High Plains aquifer is also faintly visible. Areas that disagree between analytical and geological K maps

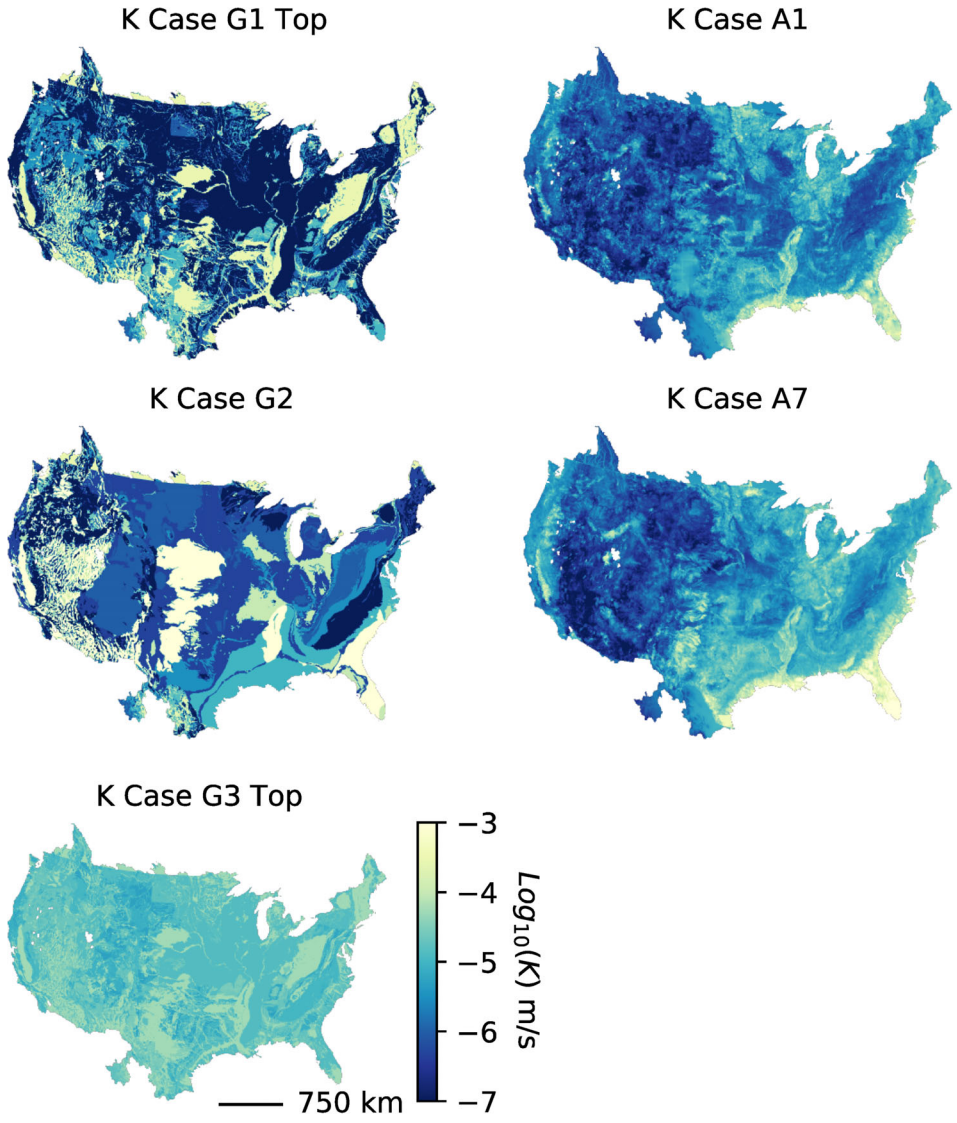

Figure 6. Comparison of analytically and geologically derived hydraulic conductivity data products. White inland areas in all products represent lakes without any estimated value of K.

Table 4
Statistical Comparison of Analytically and Geologically Derived Hydraulic Conductivity Values

	Log-Transformed Data		Untransformed Data	
Name	**Mean**	**STD**	**Mean**	**STD**
Geological K Case 1 (top layer)	−5.79	1.90	9.83E-05	1.39E-04
Geological K Case 1 (bottom layer)	−6.77	1.54	6.40E-06	2.19E-05
Geological K Case 2	−5.37	1.69	1.80E-04	3.28E-04
Geological K Case 3 (top layer)	−4.64	0.33	2.99E-05	2.02E-05
Geological K Case 3 (bottom layer)	−4.88	0.23	1.53E-05	8.81E-06
Analytical K Case 1	−5.68	0.69	9.65E-06	3.72E-05
Analytical K Case 2	−4.77	0.82	8.83E-05	2.44E-04
Analytical K Case 3	−6.01	0.70	5.09E-06	2.90E-05
Analytical K Case 4	−5.31	0.70	2.71E-05	1.13E-04
Analytical K Case 5	−4.41	0.77	1.57E-04	3.38E-04
Analytical K Case 6	−5.63	0.72	1.46E-05	7.09E-05
Analytical K Case 7	−5.45	0.79	2.77E-05	1.38E-04
Analytical K Case 8	−5.41	0.76	2.16E-05	8.80E-05
Analytical K Case 9	−3.80	0.92	3.58E-03	4.53E-02
Analytical T Case 1	−4.10	0.72	1.00E-03	1.43E-02
Analytical T Case 2	−4.06	0.65	3.11E-04	9.35E-04
Analytical T Case 3	−2.45	0.80	3.49E-02	1.90E-01

Note: Conductivities in in m/s, transmissivities in m^2/s.

include the Midwest and Basin and Range. Our large-scale mean conductivities resemble those of geology-informed approaches from literature as seen in Table 4. Figures S7 and S8 present all nine hydraulic conductivity maps and all three transmissivity maps from analytical approaches.

We find that K values derived from analytical approaches are slightly higher on average with smaller standard deviations than K values derived from geologically informed approaches (Table 4, Figure 7). The exception to this finding is *Geological K Case G3*, which has a higher mean and smaller standard deviation than the analytically derived K fields. Analytical cases 2 and 5 trend toward the highest Ks among the *Literature Analytical Approach* cases. Both of these cases assume that valley depth d was less than or equal to aquifer thickness H. This result highlights the sensitivity of the *Literature Analytical Approach* to the relationship of valley depth with aquifer thickness. *Analytical K Case 9* and *Analytical T Case 3* appear to be outliers among the *Study Analytical Approach results*. This is due to the fact that model slopes, which are calculated at a resolution of 1000 m, the resolution of the hydrologic model, instead of 250 m, were used to infer hydraulic gradient, thus decreasing slope and increasing K values. Table 4 offers a statistical comparison of all K products and Figure 7 presents the probability density functions of each analytically derived set and the probability mass function of each geologically informed product.

Hydrological Modeling Results

We make use of the UCRB ParFlow-CLM results to assess the performance of our hydraulic conductivity products in application. The results at all 10 USGS stream gages for each of our 10 simulations can be found in Figures S9 to S18. As shown in Table 3, five simulations were run without any vertical flow barrier having an effective thickness (combined thickness of model elements hydraulically connected to streams without a retarding barrier) equivalent to the full model thickness of 1192 m. We find that our models overpredict baseflow in each of these simulations (Figure 8). Regardless of overprediction, the *literature and this study's analytical approaches* perform similarly to each other, both predicting just over twice the observed values having average relative biases across all 10 stream gages of 110% and 106% respectively. These values are slightly higher than the 75% seen in the *Case G1* modeling and the 58% seen in *Case G2* but considerably less than the 652% relative bias from the *Case G3* simulation. Accuracy in timing appears to be muted in all cases by the vast overprediction of baseflow. Still, the two analytical approaches perform similarly with an average Spearman's Rho of 0.35 for both cases. The timing in *Case G1* is marginally worse with a Spearman's Rho of 0.34, *Case G3* performs worst with a Rho of 0.20, and *Case G2* performs best with a Rho of 0.44.

Our results support the idea that aquifer hydraulic conductivity is an important control on stream baseflow. We see cases with higher hydraulic conductivity values appear to display greater overprediction. This result is clear when comparing the hydrographs of our K *Case G1* simulation, which had the lowest basin-wide average K with our K *Case G3* simulation, which had the highest basin-wide average K. Here, *Case G1* overpredicts 10th-percentile flows by 230% on average across all 10 stream gages, and *Case G3* overpredicts 10th-percentile flows by 1520%. The *G2 Case* presents an anomaly in that its K values are not lower than *Case G1*, yet it predicts lower baseflows. This suggests that the spatial distribution of K along with the large-scale average has impacts on streamflows.

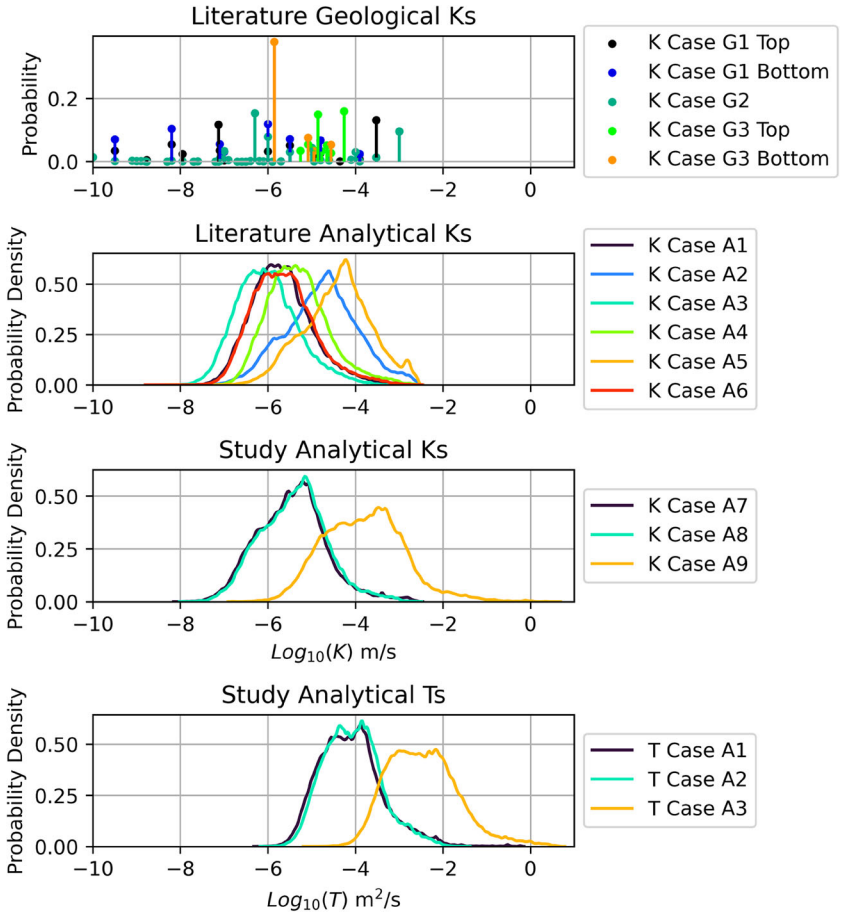

Figure 7. Probability density and mass functions of hydraulic conductivity fields. Note here that T is transmissivity and K is hydraulic conductivity. Note in this figure K Case G1 Top and K Case G1 Bottom are from the same case and represent the Top Geology and Bottom Geology portions of Figure 3. Same is true here for K Case G3 Top and K Case G3 Bottom.

The impact of effective model thickness on streamflow is illustrated when a vertical flow barrier is imposed on the model at specified depths. With the spatially variable vertical flow barrier at an estimated depth to bedrock, we see a dramatic decrease in simulated baseflow (Figure 9). However, it appears that the variable-depth vertical flow barrier has caused a systematic underprediction in streamflow for both *Case G1* with a relative bias of −30% at Lee's Ferry and *Analytical K Case A7* with a relative bias of −77% at Lee's Ferry. Our headwaters perform better with the vertical flow barrier, however. This is reflected in an arithmetic mean relative bias across all gages of −58% for the *Analytical K Case A7* Approach and 3% for *Case G1*. Additionally, we see an improvement of timing, as the Spearman's Rho our *Analytical K Case A7* Approach increases from 0.35 to 0.53, and *Case G1* improves from 0.34 to 0.49.

By comparing simulated groundwater depths with nearly 2000 annually averaged monitoring well observations, comparisons between observed and predicted WTD result in RSME values ranging from 8.9 to 12.5 m across 10 simulations. As in our surface water comparisons, the *Literature Analytical Approach* and the *Study Analytical Approach* compare similarly with RMSEs of 9.25 m and 9.24 m respectively. Our two analytical approaches outperform K *Case G1* and K *Case G3* in terms of R and R^2, but the *Geological K Case 2* map performs best overall. Correlation plots are shown in Figure 10 (without vertical flow barrier) and Figure 11 (with vertical flow barrier). The similarity in performance between Analytical cases 1 and 7 and the *Geological K Case 2* K field can be seen in their correlation coefficients and respective plots. We associate this similarity in performance with the similarity in area-weighted mean K seen between these three products.

We find that all cases and approaches underpredict groundwater depth, meaning that the elevation of the simulated water table is too high. This can be seen in Table 5, where the mean deviation between observed groundwater depths and simulated groundwater depths is positive for all cases. Our addition of vertical flow barriers improves this bias but hurts groundwater depth predictions holistically (Figure 11). It can be seen, however, that the improvement of streamflow estimates due to the vertical flow barrier is larger than the worsening of the waters table depth. Maps of predicted and observed WTD can be found for all 10 simulations in Figures S20 to S29. These K fields present the errors in observed-predicted WTD and can be used to further demonstrate the spatial distribution of this error.

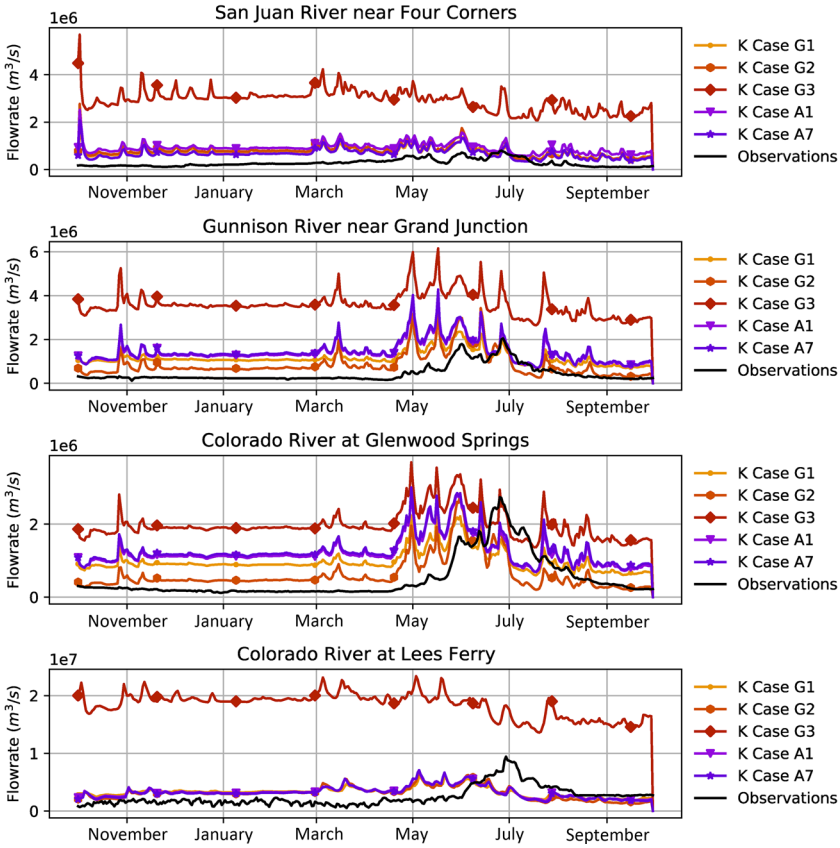

Figure 8. Hydrograph results at four representative stream gages in the UCRB.

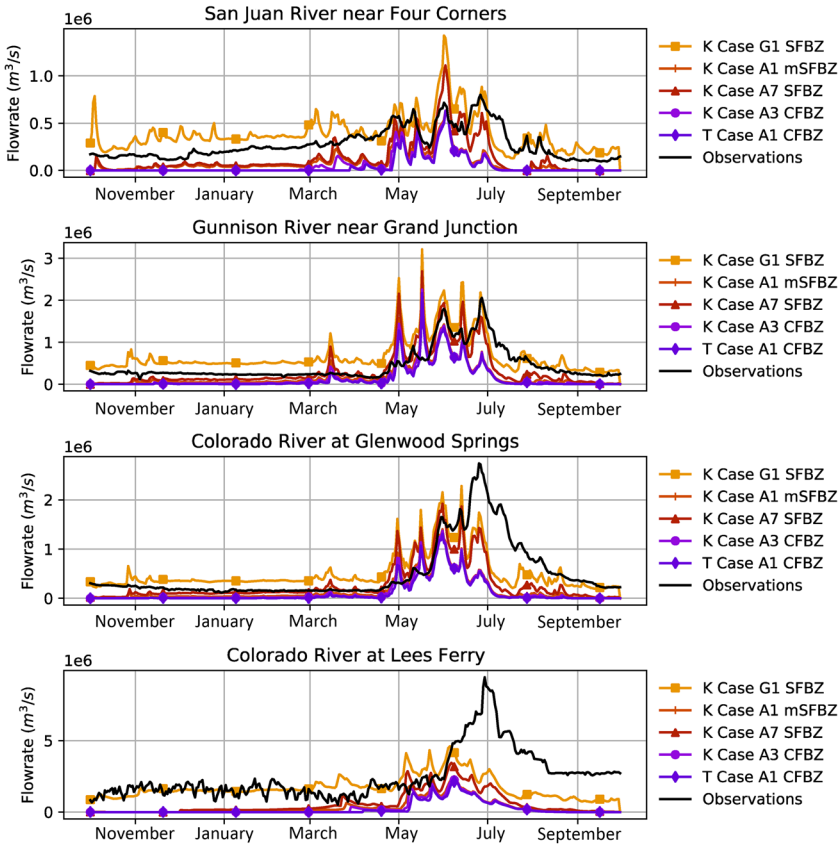

Figure 9. Hydrograph results for four selected stream gages.

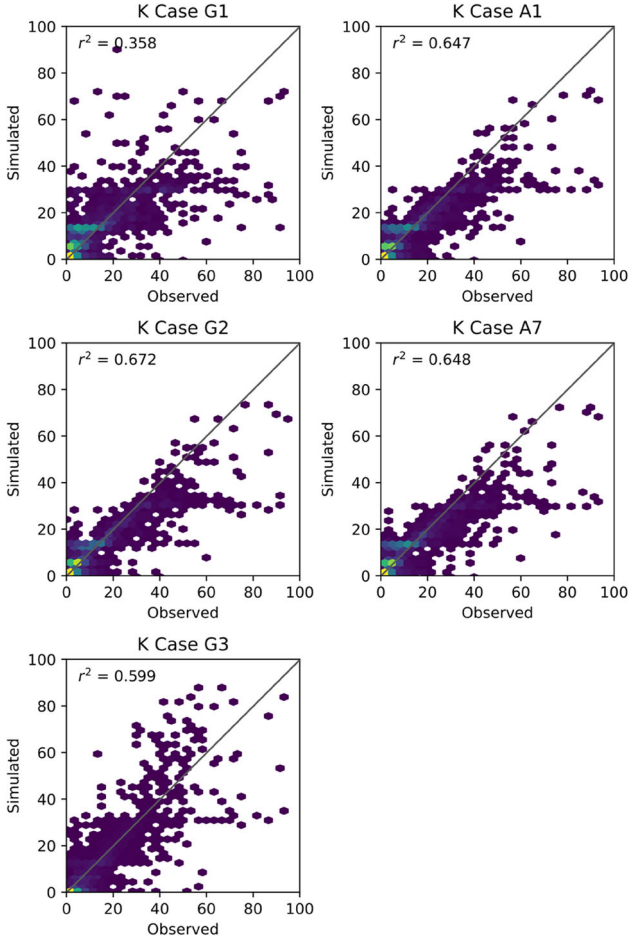

Figure 10. Density scatterplots of simulated groundwater depth and observed groundwater depth from Fan (Fan et al. 2013) in the UCRB for simulations without a vertical flow barrier. Note that colors represent the density of points that fall within a range of values, brighter colors signify that many points fall along the same location.

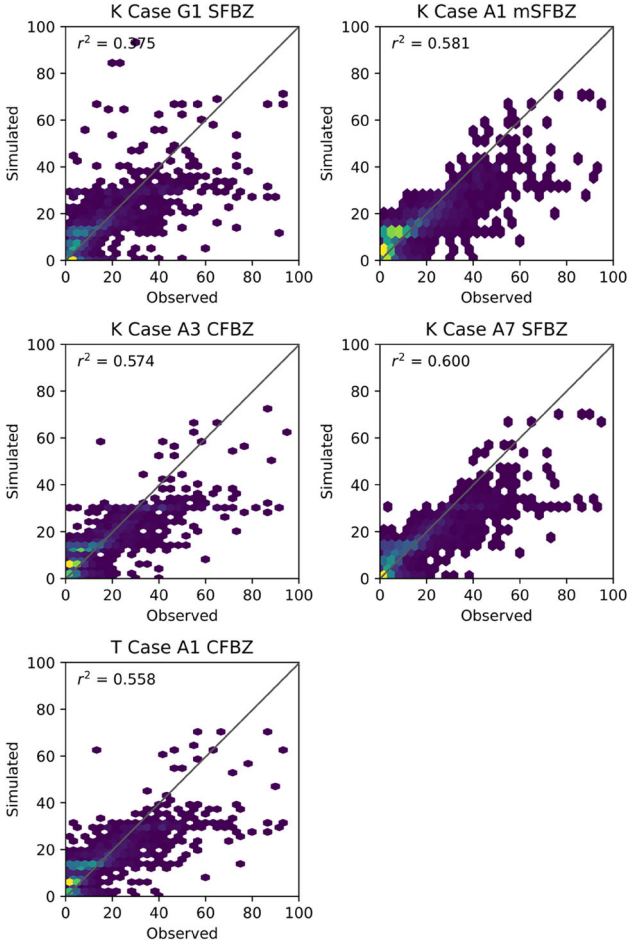

Figure 11. Density scatterplots of simulated groundwater depth and observed groundwater depth from Fan (Fan et al. 2013) in the UCRB for simulations that include a vertical flow barrier. Note that colors represent the density of points that fall within a range of values, brighter colors signify that many points fall along the same location.

Discussion

We find analytical hydraulic conductivity fields to be smoother than geologically informed ones. In the *Geological* cases the effective K values was not distributed within indicator categories as there is not much information on this at large scale. Some work suggests that distributions in K around effective values are important at smaller scales and finer resolution and that runoff processes may average up at the hillslope scale (Meyerhoff and Maxwell 2011). The Analytical Cases distribute K values throughout as each value is determined via the analytical approximation at the resolution applied, one of the reasons for conducting this comparison. This finding is consistent with groundwater finding preferential flow paths around or through geologic features with low hydraulic conductivity, such that even areas mapped with predominantly low K geologies would have a resulting higher effective K. The same could be seen in areas that have primarily high K, but poor connectivity due to low K in a few areas to bottleneck flow; although, this is less common. Higher hydraulic conductivities at larger scales have been noted in literature and are generally accepted as a naturally occurring phenomenon (Neuman 1994; Schulze-Makuch et al. 1999). Smoother transitions in K also arise from averaging the data over HUC12 regions and limitations in the input datasets. For example, analytical approaches are sensitive to stream density, which is limited by the scale at which it was mapped.

Our experiments with the vertical flow barrier suggest that the thickness of model units hydraulically connected to streams plays a large role on governing baseflow. This in turn suggests that these higher Ks would perform best in a hydrologic model with a shallower subsurface, or one with a model feature to limit baseflow like a vertical barrier. The results from our implementation of the *Literature Analytical Approach*, we see the influence of input parameters on resulting K values. For example, in *Analytical K Cases 2* and *5*, we see the sensitivity of the approach to valley depth (d). In these cases, valley depth was assumed to be less than or equal to depth to bedrock (H). This assumption forced shallower valley depths than

Table 5
Groundwater Depth Prediction Performance Statistics

Subsurface	R^2	RMSE (m)	Mean Deviation: Obs-Calc (m)
Geological K Case 1	0.40	12.5	0.24
Geological K Case 2	0.70	8.9	1.68
Geological K Case 3	0.67	9.9	1.90
Analytical K Case 1	0.68	9.3	1.52
Analytical K Case 7	0.68	9.2	1.62
Geological K Case 1 (SFBZ)	0.41	12.3	0.28
Analytical K Case 1 (mSFBZ)	0.59	10.1	0.46
Analytical K Case 7 (SFBZ)	0.62	9.8	1.55
Analytical K Case 3 (CFBZ)	0.60	10.2	0.43
Analytical T case 1 (CFBZ)	0.58	10.4	0.37

Note: CFBZ indicates a constant-depth flow barrier and SFBZ indicates a variable-depth flow barrier at Shangguan's depth to bedrock. The modified variable-depth flow barrier (mSFBZ) is located at a depth of 100 m or Shangguan's estimate of depth to bedrock, whichever is greater.

calculated by the black-top-hat transform in areas with steep topography and shallow depths to bedrock. We made this assumption to increase the number of catchments in which we could analytically calculate K (in cases where valley depth is greater than twice the bedrock depth this approach results in negative values of K, which are obviously non-physical). In *Literature Analytical Cases* 1, 3, 4, and 6, we left valley depth unchanged and made assumptions regarding bedrock depth. We see closer agreement in these cases highlighting the influence of the black-top-hat transform result on K. This transform was readily performed by existing python libraries, which make it easy to do, but choosing the parameters for the transform is less intuitive. The black-top-hat transform requires the mapper to specify a search window shape and radius, which is a difficult to infer from physical parameters.

The *Study Analytical Approach*, like the *Literature Analytical Approach*, is sensitive to input parameters as is illustrated in the cases with model slopes and flow lengths: *Analytical K Case 9* and T *Case 3*. The mathematical reason for these outliers is that we have effectively flattened the slope and increase the flow lengths in nearly all catchments. In application, the two analytical approaches explored were both doable with readily available Python tools. Topographic slope to infer hydraulic gradient may or may not be a more accurate proxy for hydraulic gradient but requires no parameter such as the black-top-hat's window size and conceptually seems to perform better in steeply contoured mountainous aquifers.

Of course, this study has limitations. The hydrologic model we used should be considered an example application case and not a perfect assessment of the physical truth. The total transmissivity of model units interacting with streams is shown to have a large impact on streamflow. We show that high K leads to higher streamflow and lower WTD. We hypothesize that this is the result of more lateral groundwater flow to streams, and less water lost to evapotranspiration (ET). While WTD is clearly linked to ET (e.g. Kollet and Maxwell 2008) K-ET relationships have mostly been demonstrated at much smaller scales (e.g. Atchley and Maxwell 2011). The high streamflow values of the *K Case G3* simulation and the lower, more accurate, streamflows of the cases with flow barriers are supportive of this. When looking at groundwater levels in comparison to observations, we see shallower predicted water tables over the majority of the domain. This systematic error could be a result of model physics, as it is constant across high and low values of K. We hypothesize that the 1 km resolution of our model may not fully capture the steep topography of the domain, resulting in lower simulated hydraulic gradients and consequently higher water tables. It is also possible that the positive errors covary with the location of the wells. This is possible if wells are preferentially drilled in specific areas with a physical reason to bias one way or another in our model. Consider that the majority of wells may likely be drilled in lowland areas where groundwater is most accessible and contributes to streamflow where streambeds have incised down to the water table. Our model simulates streams without incision, so it is likely that we see a slight shallow bias for WTD in lowland areas. A challenge in this work is that there is not a clear "winner" among the cases. Some cases have better streamflow, some better WTD and some of the cases are better for streamflow. For example, *Case G1 SFBZ* matches the flows the best but has poorer groundwater performance when compared to *Case A7 SFBZ*. These examples highlight the challenges of determining a single best subsurface over a continental scale basin.

Conclusions

This study addressed the challenge of characterizing hydraulic conductivity at the continental scale comparing both analytical and geologically informed approaches. We used an analytical approach from literature as well as novel approach derived in this study to produce nine hydraulic conductivity maps and three transmissivity maps for the contiguous United States and adjacent hydrologic regions. We compared the results of analytical approaches to each other and to hydraulic conductivity values from literature finding them to be similar in mean value, standard deviation, and in some instances, spatial trend. We tested K data products from both analytical approaches and three geology-informed approaches in a fully integrated hydrologic model of a basin-scale watershed—something unique to this study.

We found that the hydraulic conductivity of the subsurface plays a role in surface water partitioning, which highlights the interconnectedness of groundwater, soil moisture, and surface water. Specifically, we saw higher mean K values produce more simulated streamflow causing higher relative bias in the form of over-prediction, a result similar to prior studies conducted at smaller

scales (Foster and Maxwell 2019). This supports holistic approaches to conceptualizing and modeling hydrology. We found that limiting the thickness and consequently the effective transmissivity of simulated aquifer units by use of a vertical flow barrier has important impacts for surface water as well, primarily in the form of reducing baseflow, which is groundwater driven. Conversely, we found that peak flows, which were snowmelt dominated and largely runoff driven in our domain, are affected less by model subsurface configuration.

The findings of this study support the use of geomorphology and analytical approaches to make inferences about subsurface hydrostratigraphy. We found that analytical approaches yield estimates of K that produce similar streamflow and WTD statistics compared to non-analytical, geology-informed estimates from literature. We also show that the analytical approach derived by this study, referred to herein as the *Study Analytical Approach*, produces estimates of K that are similar in spatial distribution, standard deviation, mean value, and modeling performance to estimates from the *Literature Analytical Approach* (Luo et al. 2010). Moreover, the *Study Analytical Approach* required fewer assumptions in application.

Finally, we conclude that the underlying assumptions of our analytical approaches, while imperfect, may be useful for conceptualizing and modeling the subsurface at large scales. For example, we do not capture the three-dimensional heterogeneity of hydraulic conductivity, nor do we capture anisotropy. However, our approach offers utility as it has been successfully used to estimate effective hydraulic conductivity at large scales.

Acknowledgments

This research has been supported by the U.S. Department of Energy Office of Science (grant no. DE-AC02-05CH11231) and the US National Science Foundation Office of Advanced Cyberinfrastructure (grant no. OAC-2054506 and OAC-1835855). Data products will be made available via the HydroFrame project (https://hydroframe.org) upon final publication. We thank the Editor in Chief (L. Konikow), Executive Editor (M. Hill), and three anonymous reviewers for their constructive comments which have added to the quality and clarity of this work.

Authors' Note

The author(s) does not have any conflicts of interest or financial disclosures to report.

Supporting Information

Additional supporting information may be found online in the Supporting Information section at the end of the article. Supporting Information is generally *not* peer reviewed.

Data S1. Figure S1. Map of recharge for the contiguous United States from Tran et al. (2020).
Figure S2. Map of unconsolidated depth to bedrock over the contiguous United States from Shangguan et al. (2017).
Figure S3. Map of drainage density for the contiguous United States calculated from NHD Plus stream data.
Figure S4. Map of average effective flow length for the contiguous United States calculated from NHD Plus stream data.
Figure S5. Black top hat transform results over the contiguous United States. DEM processed at 30 m resolution and averaged at 250 m resolution for storage and use.
Figure S6. Topographic slope over the contiguous United States. DEM collected at 30 m resolution and averaged at 250 m resolution for storage and use.
Figure S7. Hydraulic conductivity results from the literature analytical approach.
Figure S8. Hydraulic conductivity and transmissivity results from this study's analytical approach.
Figure S9. Simulated and observed stream flows at 10 USGS stream gages within the UCRB model—subsurface: Analytical K Case 1.
Figure S10. Simulated and observed stream flows at 10 USGS stream gages within the UCRB model—subsurface: Analytical K Case 7.
Figure S11. Simulated and observed stream flows at 10 USGS stream gages within the UCRB model—subsurface: Geological K Case 1.
Figure S12. Simulated and observed stream flows at 10 USGS stream gages within the UCRB model—subsurface: Geological K Case 2.
Figure S13. Simulated and observed stream flows at 10 USGS stream gages within the UCRB model—subsurface: Geological K Case 3.
Figure S14. Simulated and observed stream flows at 10 USGS stream gages within the UCRB model—subsurface: Analytical K Case 7, with spatially variable vertical flow barrier at Shangguan's estimate of depth-to-bedrock.
Figure S15. Simulated and observed stream flows at 10 USGS stream gages within the UCRB model—subsurface: Geological K Case 1, with spatially variable vertical flow barrier at Shangguan's estimate of depth-to-bedrock.
Figure S16. Simulated and observed stream flows at 10 USGS stream gages within the UCRB model—subsurface: Analytical K Case 1, with spatially variable vertical flow barrier at Shangguan's estimate of depth-to-bedrock or 100 m, whichever is deeper.
Figure S17. Simulated and observed stream flows at 10 USGS stream gages within the UCRB model—subsurface: Analytical K Case 3, with a vertical flow barrier at a constant 192 m.
Figure S18. Simulated and observed stream flows at 10 USGS stream gages within the UCRB

model—subsurface: Analytical T Case 1, with a vertical flow barrier at a constant 192 m.

Figure S19. Percentages of domain interpolated using nearest neighbor and extrapolated using a linear ridge model form Scikit Learn.

Figure S20. Simulated water table depths in the UCRB: Geological K Case 1.

Figure S21. Simulated water table depths in the UCRB: Geological K Case 2.

Figure S22. Simulated water table depths in the UCRB: Geological K Case 3.

Figure S23. Simulated water table depths in the UCRB: Analytical K Case 1.

Figure S24. Simulated water table depths in the UCRB: Analytical K Case 7.

Figure S25. Simulated water table depths in the UCRB: Geological K Case 1 SFBZ.

Figure S26. Simulated water table depths in the UCRB: Geological K Case 1 mSFBZ.

Figure S27. Simulated water table depths in the UCRB: Geological K Case 7 SFBZ.

Figure S28. Simulated water table depths in the UCRB: Geological K Case 3 CFBZ.

Figure S29. Simulated water table depths in the UCRB: Geological T Case 1 CFBZ.

References

Ashby, S., and R. Falgout. 1996. A parallel multigrid preconditioned conjugate gradient algorithm for groundwater flow simulations. *Nuclear Science and Engineering* 124, no. 1: 145–159. https://doi.org/10.13182/NSE96-A24230

Atchley, A.L., and R.M. Maxwell. 2011. Influences of subsurface heterogeneity and vegetation cover on soil moisture, surface temperature and evapotranspiration at hillslope scales. *Hydrogeology Journal* 19: 289–305. https://doi.org/10.1007/s10040-010-0690-1

Barthel, R. 2014. A call for more fundamental science in regional hydrogeology. *Hydrogeology Journal* 22, no. 3: 507–510. https://doi.org/10.1007/s10040-014-1101-9

Belitz, K., E. Watson, T.D. Johnson, and J. Sharpe. 2019. Secondary hydrogeologic regions of the conterminous United States. *Groundwater* 57, no. 3: 367–377. https://doi.org/10.1111/gwat.12806

Bierkens, M.F.P., V.A. Bell, P. Burek, N. Chaney, L.E. Condon, C.H. David, A. de Roo, P. Döll, N. Drost, J.S. Famiglietti, M. Flörke, D.J. Gochis, P. Houser, R. Hut, J. Keune, S. Kollet, R.M. Maxwell, J.T. Reager, L. Samaniego, E. Sudicky, E.H. Sutanudjaja, N. van de Giesen, H. Winsemius, and E.F. Wood. 2015. Hyper-resolution global hydrological modelling: What is next? *Hydrological Processes* 29, no. 2: 310–320. https://doi.org/10.1002/hyp.10391

Condon, L.E., S. Kollet, M.F.P. Bierkens, G.E. Fogg, R.M. Maxwell, M.C. Hill, H.-J.H. Fransen, A. Verhoef, A.F. van Loon, M. Sulis, and C. Abesser. 2021. Global groundwater modeling and monitoring: Opportunities and challenges. *Water Resources Research* 57, no. 12: e2020WR029500. https://doi.org/10.1029/2020WR029500

Condon, L.E., and R.M. Maxwell. 2014. Feedbacks between managed irrigation and water availability: Diagnosing temporal and spatial patterns using an integrated hydrologic model. *Water Resources Research* 50, no.3: 2600–2616. https://doi.org/10.1002/2013WR014868

Condon, L.E., and R.M. Maxwell. 2013. Implementation of a linear optimization water allocation algorithm into a fully integrated physical hydrology model. *Advances in Water Resources* 60: 135–147. https://doi.org/10.1016/j.advwatres.2013.07.012

Desbarats, A.J., C.E. Logan, M.J. Hinton, and D.R. Sharpe. 2002. On the kriging of water table elevations using collateral information from a digital elevation model. *Journal of Hydrology* 255, no. 1–4: 25–38. https://doi.org/10.1016/S0022-1694(01)00504-2

Eagleson, P.S. 1986. The emergence of global-scale hydrology. *Water Resources Research* 22, no. 9S: 6S–14S. https://doi.org/10.1029/WR022i09Sp0006S

Enemark, T., L. Peeters, D. Mallants, B. Flinchum, and O. Batelaan. 2020. A systematic approach to hydrogeological conceptual model testing, combining remote sensing and geophysical data. *Water Resources Research* 56, no. 8: e2020WR027578. https://doi.org/10.1029/2020WR027578

Enemark, T., L.J.M. Peeters, D. Mallants, and O. Batelaan. 2019. Hydrogeological conceptual model building and testing: A review. *Journal of Hydrology* 569: 310–329. https://doi.org/10.1016/j.jhydrol.2018.12.007

Fan, Y., H. Li, and G. Miguez-Macho. 2013. Global patterns of groundwater table depth. *Science* 339, no. 6122: 940–943. https://doi.org/10.1126/science.1229881

Forrester, M.M., and R.M. Maxwell. 2020. Impact of lateral groundwater flow and subsurface lower boundary conditions on atmospheric boundary layer development over complex terrain. *Journal of Hydrometeorology* 21, no. 6: 1133–1160. https://doi.org/10.1175/JHM-D-19-0029.1

Foster, L.M., K.H. Williams, and R.M. Maxwell. 2020. Resolution matters when modeling climate change in headwaters of the Colorado River. *Environmental Research Letters* 15, no. 10: 104031. https://doi.org/10.1088/1748-9326/aba77f

Foster, L., and R.M. Maxwell. 2019. Sensitivity analysis of hydraulic conductivity and Manning's n parameters lead to new method to scale effective hydraulic conductivity across model resolutions. *Hydrological Processes* 33, no. 3: 332–349. https://doi.org/10.1002/hyp.13327

Freeze, R.A., and J.A. Cherry. 1979. *Groundwater*. Englewood Cliffs, NJ: Prentice-Hall.

Gleeson, T., T. Wagener, P. Döll, S.C. Zipper, C. West, Y. Wada, R. Taylor, T. Wagener, P. Döll, S.C. Zipper, C. West, Y. Wada, R. Taylor, B. Scanlon, R. Rosolem, S. Rahman, N. Oshinlaja, R. Maxwell, M.H. Lo, H. Kim, M. Hill, A. Hartmann, G. Fogg, J.S. Famiglietti, A. Ducharne, I. de Graaf, M. Cuthbert, L. Condon, E. Bresciani, and M.F.P. Bierkens. 2021. GMD perspective: The quest to improve the evaluation of groundwater representation in continental- to global-scale models. *Geoscientific Model Development* 14, no. 12: 7545–7571. https://doi.org/10.5194/gmd-14-7545-2021

Gleeson, T., N. Moosdorf, J. Hartmann, and L.P.H. van Beek. 2014. A glimpse beneath earth's surface: GLobal HYdrogeology MaPS (GLHYMPS) of permeability and porosity. *Geophysical Research Letters* 41, 3891–3898. https://doi.org/10.1002/2014GL059856

Gleeson, T., L. Smith, N. Moosdorf, J. Hartmann, H.H. Dürr, A.H. Manning, L.P.H. van Beek, and A.M. Jellinek. 2011. Mapping permeability over the surface of the Earth. *Geophysical Research Letters* 38: L02401. https://doi.org/10.1029/2010GL045565

de Graaf, I., L. Condon, and R. Maxwell. 2020. Hyper-resolution continental-scale 3-D aquifer parameterization for groundwater modeling. *Water Resources Research* 56, no. 5: e2019WR026004. https://doi.org/10.1029/2019WR026004

Gupta, S., T. Hengl, P. Lehmann, S. Bonetti, and D. Or. 2021. SoilKsatDB: global database of soil saturated hydraulic conductivity measurements for geoscience applications. *Earth System Science Data* 13, no. 4: 1593–1612. https://doi.org/10.5194/essd-13-1593-2021

Haitjema, H.M., and S. Mitchell-Bruker. 2005. Are water tables a subdued replica of the topography? *Ground Water* 43, no. 6: 781–786. https://doi.org/10.1111/j.1745-6584.2005.00090.x

Heath, R. 1983. Basic Ground-Water Hydrology. U.S. Geological Survey Water-Supply Paper 2220. 86p. https://pubs.usgs.gov/wsp/2220/report.pdf.

Hill, M.C., and C.R. Tiedeman. 2007. *Effective Groundwater Model Calibration: With Analysis of Data, Sensitivities, Predictions, and Uncertainty*. Hoboken, NJ: John Wiley & Sons, Inc.

Hornberger, G., P. Wiberg, J. Raffensperger, and P. D'Odorico. 1998. *Elements of Physical Hydrology*. United Kingdom: Johns Hopkins University Press.

Huscroft, J., T. Gleeson, J. Hartmann, and J. Börker. 2018. Compiling and mapping global permeability of the unconsolidated and consolidated earth: GLobal HYdrogeology MaPS 2.0 (GLHYMPS 2.0). *Geophysical Research Letters* 45, no. 4: 1897–1904. https://doi.org/10.1002/2017GL075860

Jackson, T.J., R. Bindlish, M.H. Cosh, T. Zhao, P.J. Starks, D.D. Bosch, M. Seyfried, M.S. Moran, D.C. Goodrich, Y.H. Kerr, and D. Leroux. 2012. Validation of soil moisture and ocean salinity (SMOS) soil moisture over watershed networks in the U.S. *IEEE Transactions on Geoscience and Remote Sensing* 50(5 Part 1): 1530–1543. https://doi.org/10.1109/TGRS.2011.2168533

Jarvis, N., J. Koestel, I. Messing, J. Moeys, and A. Lindahl. 2013. Influence of soil, land use and climatic factors on the hydraulic conductivity of soil. *Hydrology and Earth System Sciences* 17, no. 12: 5185–5195. https://doi.org/10.5194/hess-17-5185-2013

Jones, J., and C. Woodward. 2001. Newton-Krylov methods for variably saturated flow. *Advances in Water Resources* 24: 763–774.

King, F.H. 1899. Principles and conditions of the movements of ground water. In *U.S. Geological Survey Nineteenth Annual Report, Part II*, 39660921. Washington, DC: Govt. Printing Office.

Kollet, S.J., and R.M. Maxwell. 2008. Capturing the influence of groundwater dynamics on land surface processes using an integrated, distributed watershed model. *Water Resources Research* 44: W02402. https://doi.org/10.1029/2007WR006004

Kollet, S.J., and R.M. Maxwell. 2006. Integrated surface-groundwater flow modeling: A free-surface overland flow boundary condition in a parallel groundwater flow model. *Advances in Water Resources* 29, no. 7: 945–958. https://doi.org/10.1016/j.advwatres.2005.08.006

Luo, W., B.P. Grudzinski, and D. Pederson. 2010. Estimating hydraulic conductivity from drainage patterns-a case study in the Oregon Cascades. *Geology* 38, no. 4: 335–338. https://doi.org/10.1130/G30816.1

Luo, W., and D.T. Pederson. 2012. Hydraulic conductivity of the High Plains Aquifer re-evaluated using surface drainage patterns. *Geophysical Research Letters* 39, no. 2: 1–6. https://doi.org/10.1029/2011GL050200

Marshall, S.K., P.G. Cook, C.T. Simmons, L.F. Konikow, and S. Dogramaci. 2022. An approach to include hydrogeologic barriers with unknown geometric properties in groundwater model inversions. *Water Resources Research* 58, no. 7: e2021WR031458. https://doi.org/10.1029/2021WR031458

Maxwell, R.M. 2013. A terrain-following grid transform and preconditioner for parallel, large-scale, integrated hydrologic modeling. *Advances in Water Resources* 53, no. March: 109–117. https://doi.org/10.1016/j.advwatres.2012.10.001

Maxwell, R.M., and L.E. Condon. 2016. Connections between groundwater flow and transpiration partitioning. *Science* 353, no. 6297: 377–380. https://doi.org/10.1126/science.aaf7891

Maxwell, R.M., L.E. Condon, and S.J. Kollet. 2015. A high-resolution simulation of groundwater and surface water over most of the continental US with the integrated hydrologic model ParFlow v3. *Geoscientific Model Development* 8, no. 3: 923–937. https://doi.org/10.5194/gmd-8-923-2015

Maxwell, R.M., and N.L. Miller. 2005. On the development of a coupled land surface and groundwater model. *Developments in Water Science* 55(PART 2): 1503–1510. https://doi.org/10.1016/S0167-5648(04)80161-8

Meyerhoff, S., and R.M. Maxwell. 2011. Quantifying the effects of subsurface heterogeneity on hillslope runoff using a stochastic approach. *Hydrogeology Journal* 19, no. 8: 1515–1530. https://doi.org/10.1007/s10040-011-0753-y

Montzka, C., M. Herbst, L. Weihermüller, A. Verhoef, and H. Vereecken. 2017. A global data set of soil hydraulic properties and sub-grid variability of soil water retention and hydraulic conductivity curves. *Earth System Science Data* 9, no. 2: 529–543. https://doi.org/10.5194/essd-9-529-2017

Neuman, S.P. 1994. Generalized scaling of permeabilities: Validation and effect of support scale. *Geophysical Research Letters* 21, no. 5: 349–352. https://doi.org/10.1029/94GL00308

O'Neill, M.M.F., D.T. Tijerina, L.E. Condon, and R.M. Maxwell. 2021. Assessment of the ParFlow–CLM CONUS 1.0 integrated hydrologic model: Evaluation of hyper-resolution water balance components across the contiguous United States. *Geoscientific Model Development* 14, no. 12: 7223–7254. https://doi.org/10.5194/gmd-14-7223-2021

O'Neill, P., R. Bindlish, S. Chan, J. Chaubell, E. Njoku, and T. Jackson. 2020. Soil Moisture Active Passive (SMAP) Algorithm Theoretical Basis Document Level 2 & 3 Soil Moisture (Passive) Data Products. https://openlandmap.org.

Pederson, D.T. 2001. Stream piracy revisited: A groundwater-sapping solution. *GSA Today* 11: 4–10.

Pedregosa, F., G. Varoquaux, A. Gramfort, V. Michel, B. Thirion, O. Grisel, M. Blondel, P. Prettenhofer, et al. 2011. Scikit-learn: Machine learning in Python. *Journal of Machine Learning Research* 12: 2825–2830.

Rahmati, M., L. Weihermüller, J. Vanderborght, Y.A. Pachepsky, L. Mao, S.H. Sadeghi, N. Moosavi, H. Kheirfam, C. Montzka, K. Van Looy, B. Toth, Z. Hazbavi, W. Al Yamani, A.A. Albalasmeh, M.Z. Alghzawi, R. Angulo-Jaramillo, A.C.D. Antonino, G. Arampatzis, R.A. Armindo, et al. 2018. Development and analysis of the Soil Water Infiltration Global database. *Earth System Science Data* 10, no. 3: 1237–1263. https://doi.org/10.5194/essd-10-1237-2018

Rodriguez, F., E. Maire, P. Courjault-Radé, and J. Darrozes. 2002. The Black Top Hat function applied to a DEM: A tool to estimate recent incision in a mountainous watershed (Estibère Watershed, Central Pyrenees). *Geophysical Research Letters* 29, no. 6: 2–5. https://doi.org/10.1029/2001GL014412

Scanlon, B.R., Z. Zhang, H. Save, A.Y. Sun, H.M. Schmied, L.P.H. van Beek, D.N. Wiese, et al. 2018. Global models underestimate large decadal declining and rising water storage trends relative to GRACE satellite data. *Proceedings of the National Academy of Sciences of the United States of America* 115, no. 6: E1080–E1089. https://doi.org/10.1073/pnas.1704665115

Schulze-Makuch, D., D.A. Carlson, D.S. Cherkauer, and P. Malik. 1999. Scale dependency of hydraulic conductivity in heterogeneous media. *Ground Water* 37, no. 6: 904–919. https://doi.org/10.1111/j.1745-6584.1999.tb01190.x

Shangguan, W., T. Hengl, J. Mendes de Jesus, H. Yuan, and Y. Dai. 2017. Mapping the global depth to bedrock for land surface modeling. *Journal of Advances in Modeling Earth Systems* 9, no. 1: 65–88. https://doi.org/10.1002/2016MS000686

Soil Survey Staff. n.d. Web Soil Survey – Natural Resources Conservation Service, United States Department of Agriculture, https://websoilsurvey.nrcs.usda.gov/ (accessed February 8, 2020).

Tapley, B.D., S. Bettadpur, M. Watkins, and C. Reigber. 2004. The gravity recovery and climate experiment: Mission overview and early results. *Geophysical Research Letters* 31, no. 9: 1–4. https://doi.org/10.1029/2004GL019920

Tashie, A., T. Pavelsky, L. Band, and S. Topp. 2021. Watershed-scale effective hydraulic properties of the continental United States. *Journal of Advances in Modeling Earth Systems* 13, no. 6. https://doi.org/10.1029/2020MS002440

Tran, H., J. Zhang, J.-M. Cohard, L. Condon, and R. Maxwell. 2020. Simulating groundwater-streamflow connections in the Upper Colorado River Basin. *Groundwater* 58: 392–405. https://doi.org/10.1111/gwat.13000

Turner, A.K. 1992. *Three-Dimensional Modeling with Geoscientific Information Systems*, 443. Dordrecht: Springer Dordrecht. https://doi.org/10.1007/978-94-011-2556-7

U.S. Geological Survey. 2019. *Attributes for NHDPlus Catchments (Version 1.1) for the Conterminous United States: Hydrologic Landscape Regions*. Reston, Virginia: Data Series.

Velpuri, N.M., G.B. Senay, and J.T. Morisette. 2015. Evaluating new SMAP soil moisture for drought monitoring in the rangelands of the US high plains. *Rangelands* 38, no. 4: 183–190. https://doi.org/10.1016/j.rala.2016.06.002

Xia, Y., C. Peter-Lidard, M. Huang, H. Wei, and M. Ek. 2014. Improved NLDAS-2 Noah-simulated hydrometeorological products with an interim run. *Hydrological Processes* 29: 780–792. https://doi.org/10.1002/hyp.10190

Zell, W.O., and W.E. Sanford. 2020. Calibrated simulation of the long-term average surficial groundwater system and derived spatial distributions of its characteristics for the contiguous United States. *Water Resources Research* 56, no. 8: e2019WR026724. https://doi.org/10.1029/2019WR026724

Zhang, J., L.E. Condon, H. Tran, and R.M. Maxwell. 2021. A national topographic dataset for hydrological modeling over the contiguous United States. *Earth System Science Data* 13, no. 7: 3263–3279. https://doi.org/10.5194/essd-13-3263-2021